11 REX-ISOLDE LINAC energy upgrade: superconducting option

Matteo Pasini

11.1 Introduction

The development of the physics programme for the REX-ISOLDE [1] facility demands an upgrade in energy and beam quality. In order to meet the energy specifications while maintaining at the same time the transverse and the longitudinal beam quality, we propose a superconducting LINAC based on quarter wave resonators which can be installed downstream of the present LINAC and will eventually replace some of the existing accelerating structure. The energy upgrade will happen in three stages; in the first stage the final energy will be limited to 5.5 MeV/u with an energy variability between 2 and 5.5 MeV/u. In the second stage the final energy will be incremented up to 10 MeV/u, and in the final stage the present low-energy section from 1.2 MeV/u will be replaced with superconducting cavities. The final stage will allow deceleration and transportation of the beam to energies lower than 1.2 MeV/u thereby increasing the possible uses of the machine.

Currently, the REX LINAC delivers beams with a mass-to-charge ratio of $3 \leq A/q \leq 4.5$ at a final energy of 3 MeV/u by means of a combination of several normal-conducting structures. After the charge breeding the first acceleration stage is provided by a 101.28 MHz 4-rod RFQ which brings the beam from an energy of 5 keV/u up to 300 keV/u. The beam is then rebunched into the first 101.28 MHz IH tank which increases the energy to 1.2 MeV/u. Three split ring cavities are used to give further acceleration to 2.2 MeV/u, then a 202.58 MHz 9-gap IH-type cavity is used to boost and to vary the energy between $2 \leq E \leq 3$ MeV/u. Figure 11.1 shows the scheme of the present LINAC.

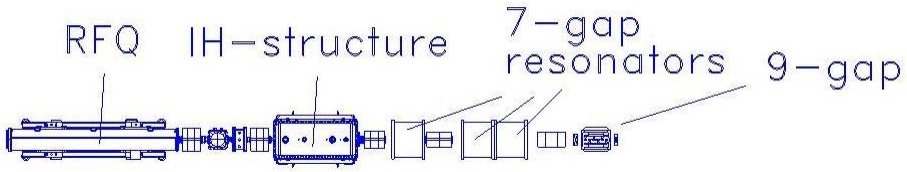

Fig. 11.1: Scheme of the REX-ISOLDE accelerator

11.2 Superconducting cavities

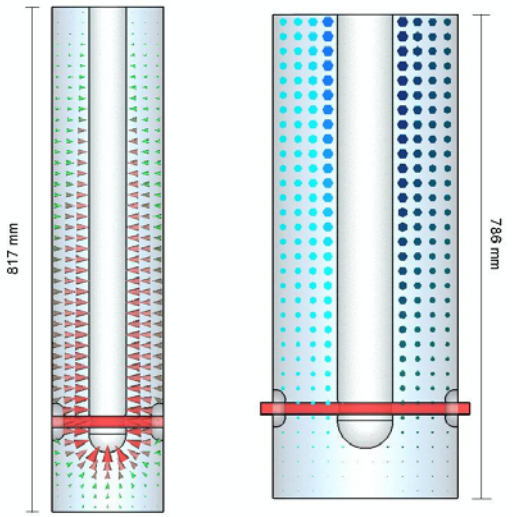

Fig. 11.2: Model of the RF quarter-wave cavities used for the LINAC simulations. On the left the cavity is represented with the electric field, on the right the magnetic field is shown.

We have chosen two-gap quarter-wave resonators as building element of the LINAC. The reduced number of gaps assures both a very high flexibility in terms of velocity acceptance and at the same time a small number of different cavity types necessary to cover the whole energy range. The energy range between 1.2 MeV/u and 10 MeV/u corresponds to a reduced velocity β between 5.1% and 14.5%. Energy of 5.5 MeV/u corresponds to a reduced velocity β = 10.8%. A first design attempted to define a geometry that could cover the velocity range required in the first stage. Figure 11.2 shows the model used for calculating the RF parameters. The cavity on the left will cover the energy gain between 1.2 and 5.5 MeV/u while the cavity on the right is designed for the higher energy section.

The first stage cavity parameters are given in Table 11.1.

Table 11.1: Cavity design parameter for the first stage scenario

No. gaps	2
β_0 (%)	7.55
f (MHz)	101.28
$\beta_0\lambda/2$ (mm)	111.74
$\lambda/4$ (mm)	740
Inner conductor diameter (mm)	60
Outer conductor diameter (mm)	180
Mechanical length (mm)	240
Gap length (mm)	40
Beam aperture diameter (mm)	20

For the second stage of the upgrade a high-beta cavity was designed. The optimized geometry is listed in Table 11.2.

Table 11.2: Cavity design parameter for the second stage scenario

No. gaps	2
β_0 (%)	12.14
f (MHz)	101.28
$\beta_0\lambda$ /2 (mm)	179.67
$\lambda/4$ (mm)	740
Inner conductor diameter (mm)	90
Outer conductor diameter (mm)	300
Mechanical length (mm)	360
Gap length (mm)	85
Beam aperture diameter (mm)	20

Figure 11.3 shows the acceleration efficiency as a function of the reduced velocity for the two cavity designs.

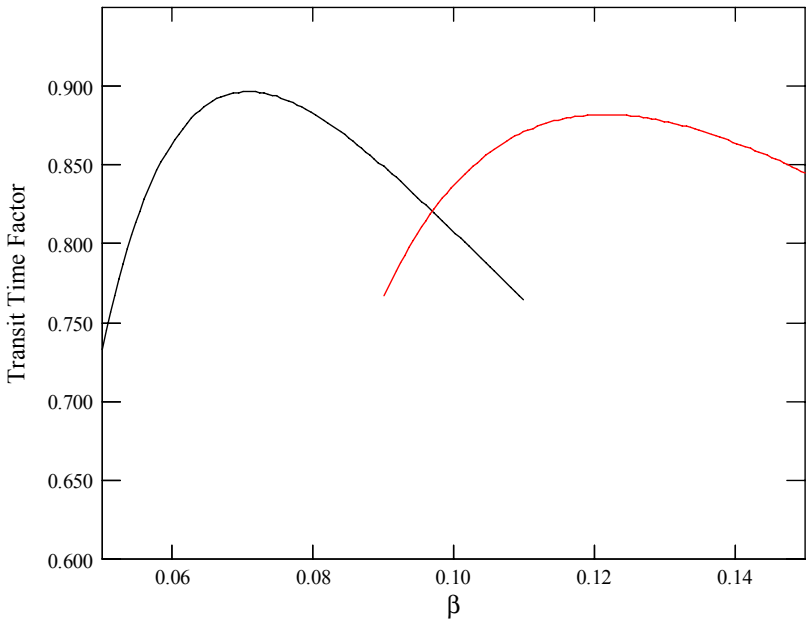

Fig 11.3: Transit time factor of the two cavities as a function of the reduced velocity β

The RF cavities should give 6 MV/m as an effective accelerating gradient (E_0T) with a power dissipation less then 7 W. The active lengths are 180 mm for the low-beta cavity and 300 mm for the high-beta one. This means a total of 1.08 MV and 1.8 MV of voltage gain, respectively, at the optimum velocity. From the transit time factor curve it is possible to calculate the energy for different masses. Figure 11.4 shows the final energy of beams with different A/q as a function of the cavity number.

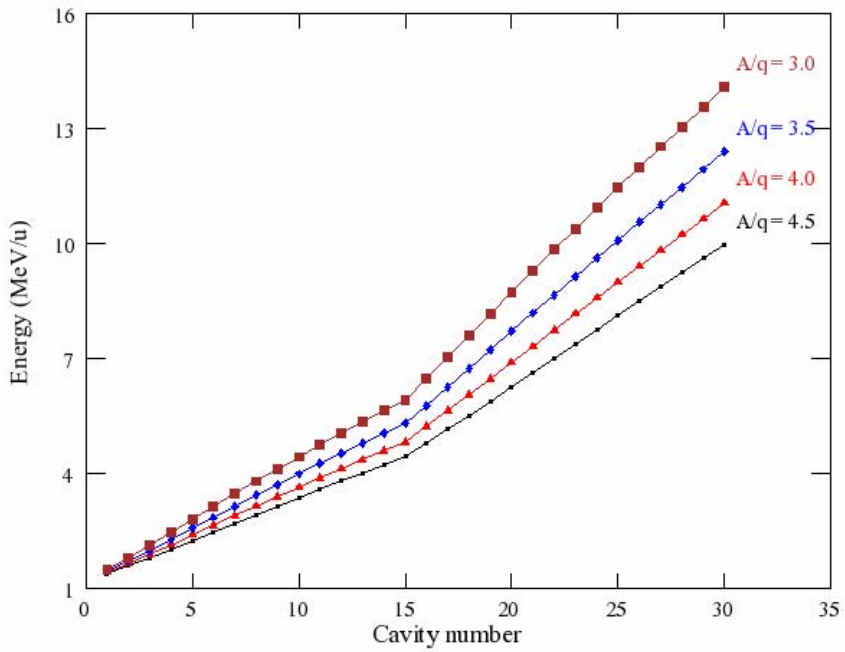

Fig. 11.4: Beam energy as a function of the cavity number for different masses (i.e., A/q)

Table 11.3 shows the derived parameters for both the geometries.

Table 11.3: RF parameters of the cavity

	Low-β cavity	**High-β cavity**
U/E_a [J/(MV/m)^2]	0.0278	0.257
E_p/E_a (#)	5.4	7.2
H_p/E_a [Oe/MV/m]	106	128
R_{sh}/Q (Ohm)	519.5	545.5
Q_0 at 6 MV/m at 7 W	3.2×10^8	4.7×10^8
TTF max	0.9	0.88

11.3 Superconducting technology

For the quarter-wave cavity there are two different types of technology that can be used for the production of the cavity itself. The first one is based on sheets of 3 mm of high grade niobium. The shape can be obtained by deep-drawing, rolling, hydro-forming etc. and all the parts are electron-beam welded. An external vessel is also made in order to contain the liquid helium. This technology is in general referred to as bulk niobium.

The other technology is based on a copper cavity where a layer of a few microns of niobium is deposited via a sputtering technique. In this case only the internal conductor is cooled directly by liquid helium since the excellent thermal conductivity of the copper assures a homogeneous temperature distribution in the cavity. This technology is in general referred to as sputtered niobium.

From the RF point of view the performance of the cavities built with the two technologies is very similar [2]; high gradients are achievable in both cases with the only noticeable difference being that mechanical stability and hence RF stability is much higher in the sputtered cavities. On the other hand, the technologies for building bulk niobium cavities are already available in industry while the sputtering technology for this kind of geometry is available in only a few laboratories (INFN-LNL, Beijing University). Figure 11.5 shows an example of the two technologies available for superconducting quarter-wave cavities.

Fig. 11.5: Photographs of the cavities made with the two technologies. The bulk niobium [3] at left and the sputtered niobium at right [4].

11.4 LINAC lattice

The roadmap of the LINAC design was to make the machine as compact as possible in order to save more space for the experiments. In general, for reasons of economy one would aim to install as many cavities as possible per cryostat; the number of cavities is limited by the transverse optics; hence if one chooses to install focusing lenses inside the cryostat, the limitation disappears. We have chosen to install five cavities per cryostat in order to establish a compromise between the economics and the complexity/difficulty of building a long cryostat. Another aspect was to reduce the distance between accelerating cavities, in order to increase the longitudinal acceptance. This is the key parameter to keep the longitudinal emittance growth small in the presence of a large initial emittance, $> 4\pi$ keV/u ns and a small synchronous phase $\phi_s = -20$ deg. The choice of superconducting solenoids seems to provide a good compromise between the beam dynamics requirements, the ease of tuning, and the increased complexity of the cryostat.

Two different cryomodule layouts have now been specified (see Fig. 11.6), one for each type of cavity. The internal cryostat layout is kept constant to reduce the cost of the design of different cryostats. Diagnostic boxes are positioned between cryomodules at the waist position in the transverse dynamics.

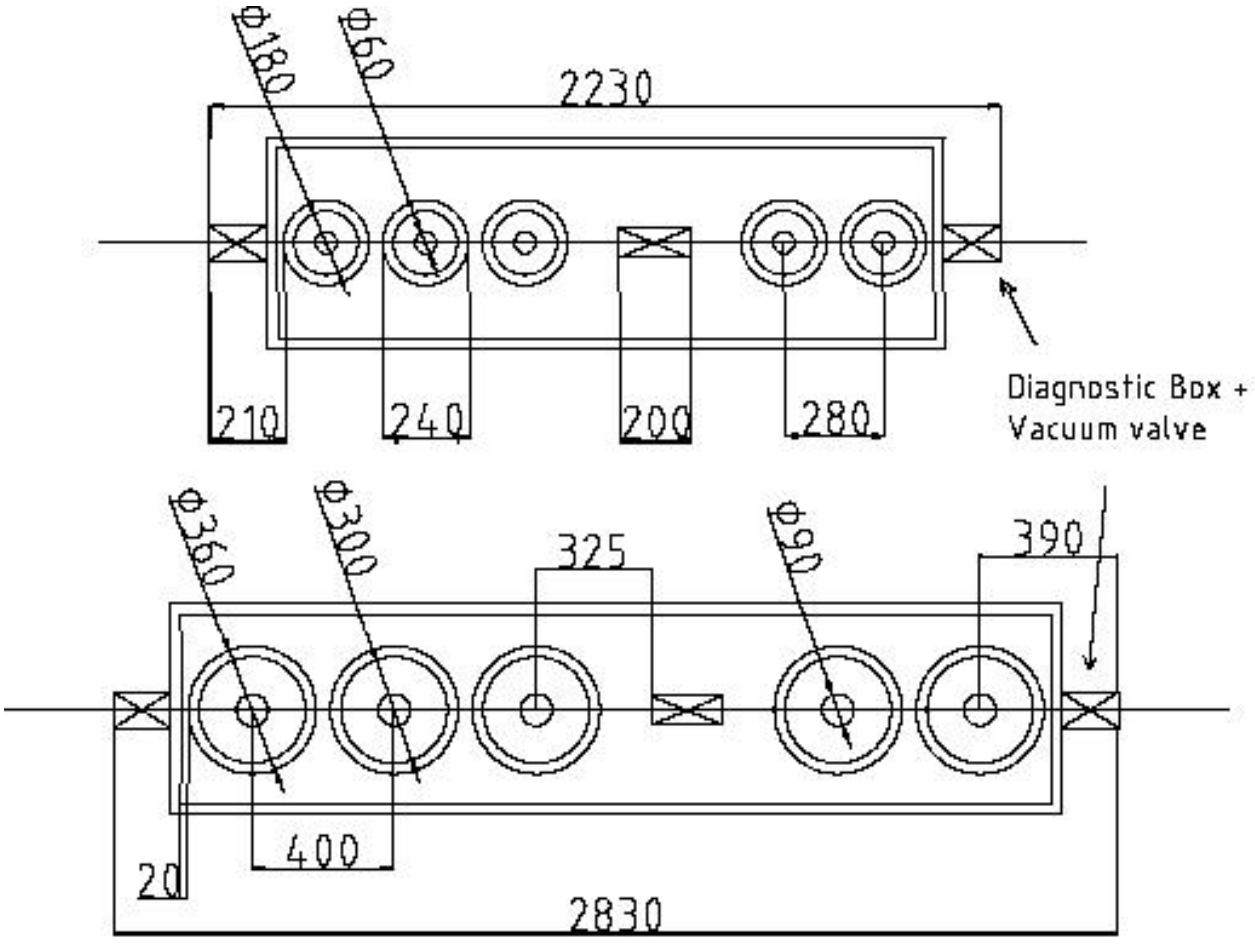

Fig. 11.6: Proposed cryomodule layout for the two different sections of the Rex LINAC energy up-grade

11.5 Beam dynamics studies

The accelerator beam dynamics were simulated using the multiparticle code LANA [5]. The simulations included only the accelerating part of the superconducting LINAC. The matching from the upstream normal-conducting section has been calculated with TRACE3D [6]. Thus far we have considered a 'square field' distribution for the cavities as well for the solenoids, so the dipole component due to the magnetic field on the beam axis has not been taken into account. Likewise, misalignment of solenoids and cavities were not considered. Beam dynamics simulations have been performed only for the complete installation so as to demonstrate the full energy variability of the superconducting machine. Input emittances are $\varepsilon_t = 0.3\,\pi$ mm mrad for the transverse plane and $\varepsilon_l = 4.5\,\pi$ keV/u ns for the longitudinal one.

The results of first-order simulations show that the emittance growth is always below 10% both in the transverse and longitudinal plane. The actual growth is located only in the first cryomodule, so a dedicated lattice can be applied at low energy. The simulations show also that it is possible to use the superconducting cavities as de- or re-bunchers, avoiding the installation of other cavities. The longitudinal beam quality can be controlled very precisely increasing at the same time the quality of the experiment.

Figure 11.7 gives an example of the beam dynamic calculation for the case of $A/q = 4.5$ and full acceleration. Figure 11.8 gives the particle distribution in the three planes at the injection and exit of the LINAC.

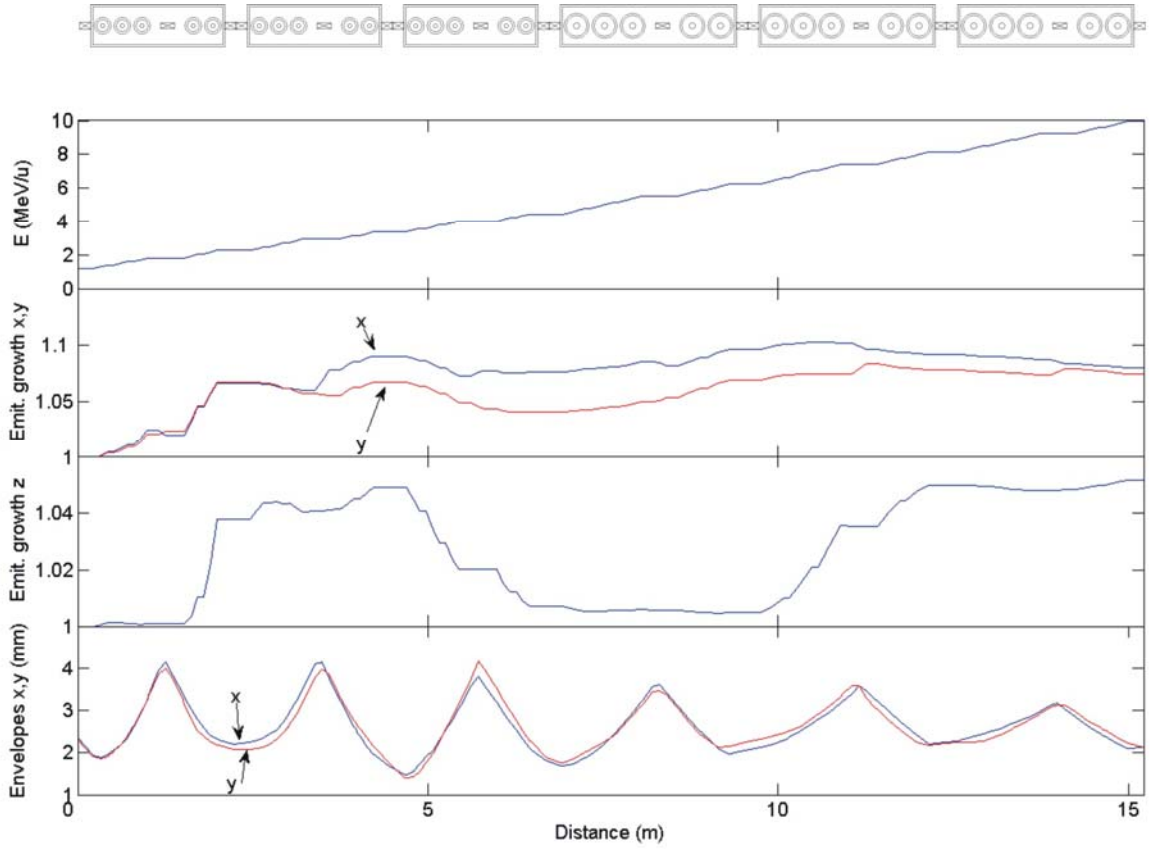

Fig. 11.7: Summary of the beam dynamics calculation of the REX energy upgrade for beams with $A/q = 4.5$. Beam parameters are shown as a function of length; from the top are shown the energy increase, the transverse (x,y) emittance growth (initial emittance was $\varepsilon_t = 0.3\pi\,\mu$m), the longitudinal emittance growth (initial emittance was $\varepsilon_l = 4.6\pi$ keV/u ns) and lastly, the envelopes x,y.

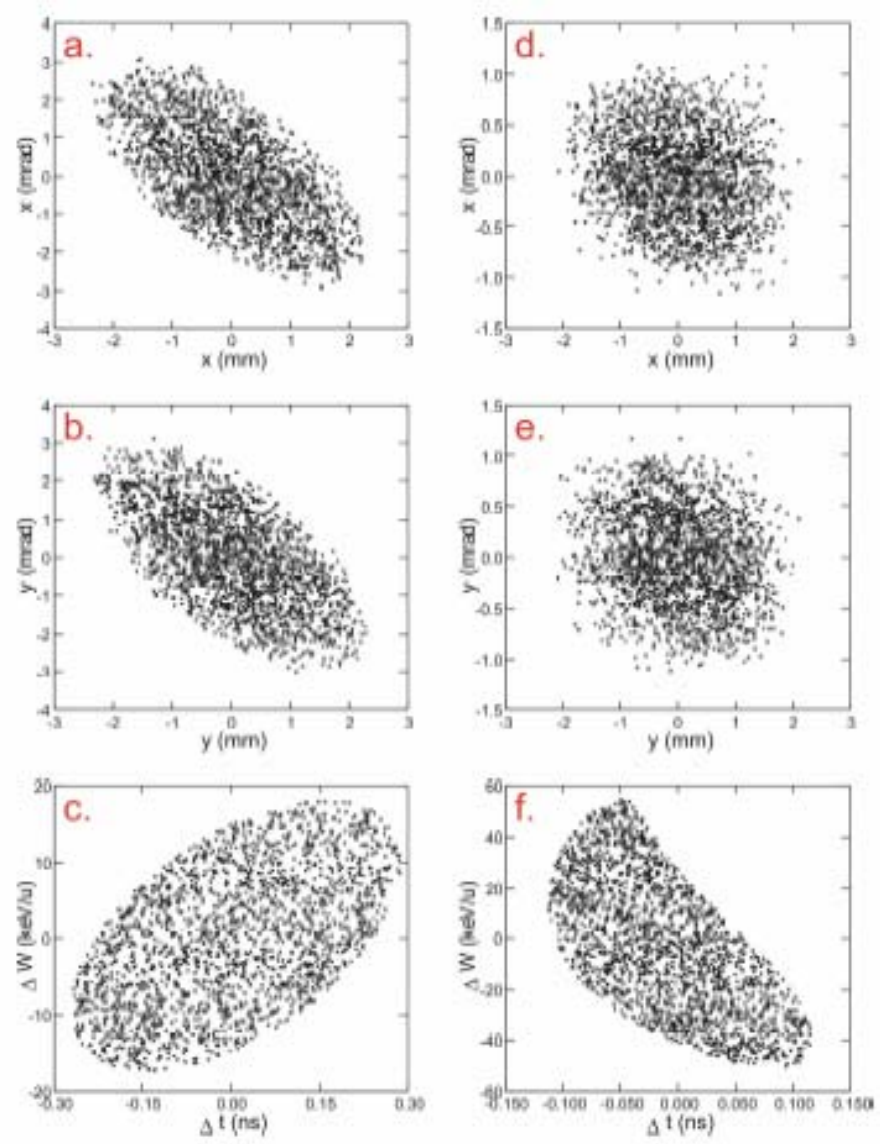

Fig. 11.8: (a), (b), (c) show the phase space portraits in the horizontal, vertical and longitudinal plane at the injection of the superconducting LINAC. Figures (d), (e) and (f) show the phase space at the exit (case with $A/q = 4.5$, $E_f = 10$ MeV/u).

11.6 Installation layout

The new extension hall provides an additional space of around 23 × 17 m. The magnetic rigidity for a beam of 10 MeV/u with $A/q = 4.5$ is about 2 Tm, and in order to optimize the space availability, large bending angles are necessary. Figure 11.9 shows a first design of the transport line to the experimental stations. At present three beam-lines are requested, leaving about seven meters from the internal wall to the extension of the accelerator. In the present scenario, beam measurement lines should be common to the transport line to the experiment. This implies also some flexibility from the optics so that, for example, an achromatic section can be used as energy spectrometer. As for the cryogenic services, the cold box can be installed in the new extension hall attached to the concrete shielding blocks that protect mostly from the high-energy X-rays. (Should there be a lack of space, lead panels could be used.) In this way the static losses due to the distribution line are reduced. Helium tank Dewar and compressors need to be installed outside the building and they would require a surface of about 60−70 m^2. As for the RF amplifiers and for the power supply, they would be put in the air-conditioned room where five 101.28 MHz and one 202.58 tube amplifiers are now running.

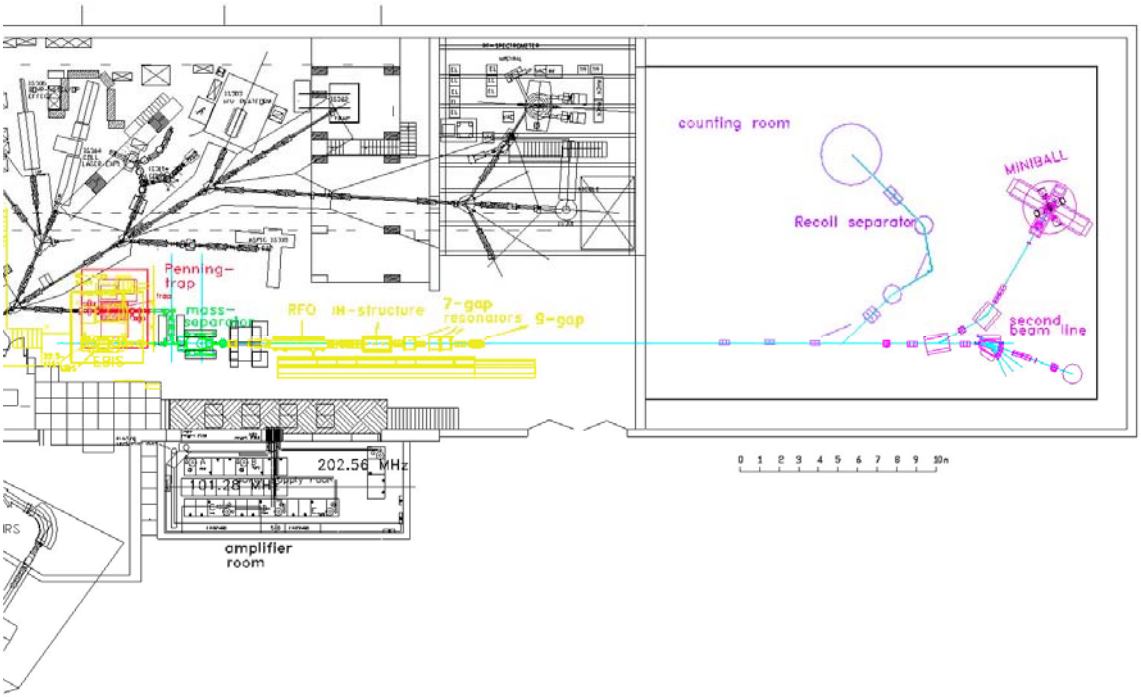

Fig. 11.9: Layout of the present installation with the foreseen beam lines in the experimental hall

Figure 11.10 shows the complete second stage for the energy upgrade, i.e., the SC LINAC starts at 1.2 MeV/u and the final energy is 10 MeV/u. The required number of cavities is 30 to be installed in 6 cryostats. This solution protrudes 3.2 m into the new experimental hall.

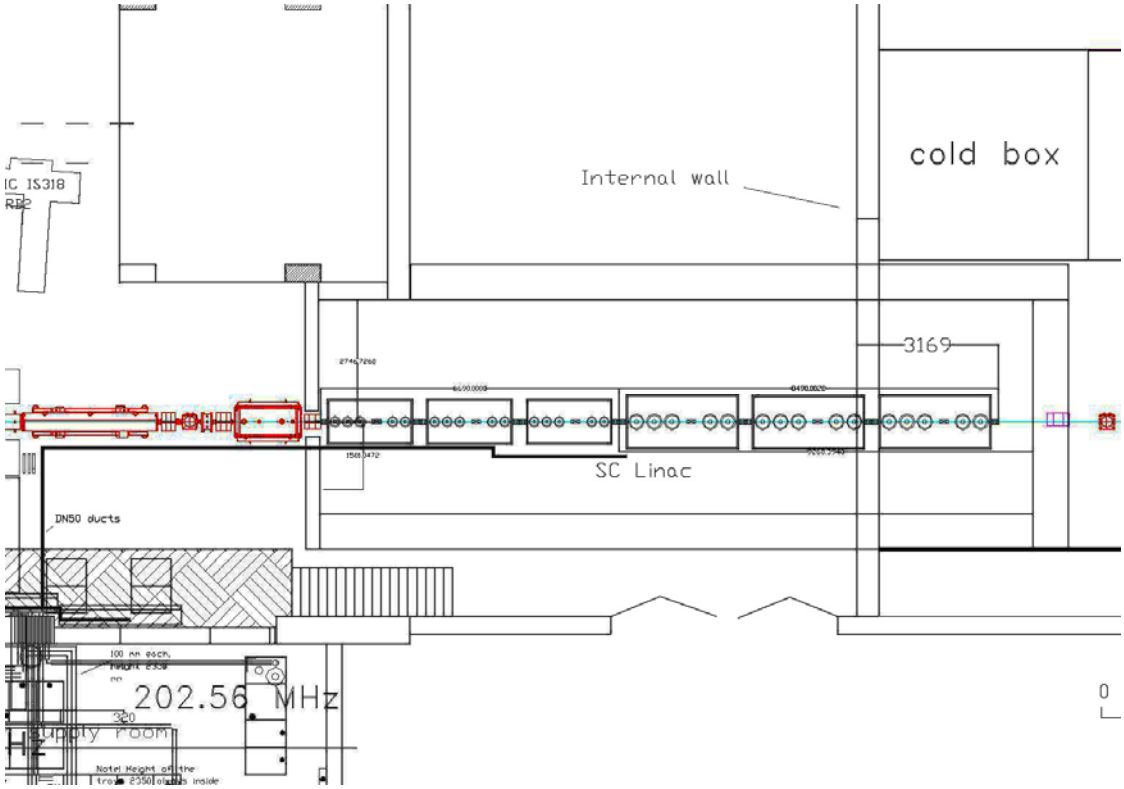

Fig. 11.10: Layout of the full installation for the SC LINAC from 1.2 to 10 MeV/u

References

[1] A. Mengoni, F. Kappeler and E. Gonzales Romero (Eds.), n TOF-Ph2, CERN-INTC-2005-21, (2005).

[2] A. Facco, Low and medium beta SC cavities, Proc. EPAC 2004 Paris, France.

[3] www.lns.cornell.edu/public/SRF2005/talks/monday/MoP06 talk srf2005.pdf

[4] www.lns.cornell.edu/public/SRF2005/talks/monday/MoP04 talk srf2005.pdf

[5] D. Gorelov and P. Ostromov, Application of LANA code for design of ion LINAC, Proc. of EPAC 1996, Sitges, e-proc1271.

[6] K.R. Crandall *et al.*, Trace 3-D Documentation, LA-UR-97-886.